# Multiple Frequency Shifting and Its Application to Accurate Multi-Scale Modeling of Induction Machine

Yue Xia, *Member, IEEE*, Peng Zhao, Kai Strunz, *Senior Member, IEEE*, Ying Chen, *Senior Member, IEEE*, and Yufei Jin

***Abstract*—The use of the shift frequency as a simulation parameter has been widely acknowledged as an enabler for multi-scale modeling of electrical power systems. So far, the frequency shifting concept has been applied to modeling electrical components considering one shift frequency. This letter aims to complement the previous work and present a multiple-frequency shifting modeling methodology. The methodology is applied to the high-slip induction machine. Two major achievements are introduced: 1) Application of frequency shifting concept for components considering multi-carriers. The Fourier spectra of machine stator and rotor quantities are shifted by different shift frequencies. 2) Modeling of components with time-varying shift frequencies. The frequency shifting modeling methodology is so extended to a wider application area. Case studies are included to demonstrate the effectiveness of the proposed method and the developed machine model.**

***Index Terms*—Induction machine, multiple shift frequencies, frequency shifting, time-varying shift frequency.**

## I. Introduction

THE electromagnetic transient program (EMTP) based on Dommel's algorithm is widely used for simulating electromagnetic transient phenomena in power systems. In EMTP, small time steps are required for tracking the ac carrier. This results in a considerable increase in computational cost when simulating electromechanical transients whose frequencies are of the order of 1 Hz and which modulate the carrier at 50 or 60 Hz. The modeling technique based on frequency shifting was proposed to achieve computational efficiency in the simulation of such low-frequency transients [1], [2]. The shift frequency is introduced as a novel simulation parameter in addition to time step size. When the shift frequency is set equal to the ac carrier frequency, the ac carrier is eliminated and larger time step sizes can be chosen. The technique was proven valuable in [3], [4] for the modeling of ac machines.

Manuscript received 20 February 2023; revised 9 August 2023 and 5 October 2023; accepted 22 October 2023. Date of publication 27 October 2023; date of current version 26 December 2023. This work was supported by the National Natural Science Foundation of China under Grant 52007194. Paper no. PESL-00064-2023. *(Corresponding author: Yue Xia.)*

Yue Xia, Peng Zhao, and Yufei Jin are with the College of Information and Electrical Engineering, China Agricultural University, Beijing 100083, China (e-mail: yue.xia@cau.edu.cn; zpengxm@163.com; 348543767@qq.com).

Kai Strunz is with the SENSE Laboratory, Department of Electrical Engineering and Computer Sciences, Technische Universität Berlin, 10587 Berlin, Germany (e-mail: kai.strunz@tu-berlin.de).

Ying Chen is with the Electrical Engineering, Tsinghua University, Beijing 100084, China (e-mail: chen_ying@tsinghua.edu.cn).

Color versions of one or more figures in this article are available at https://doi.org/10.1109/TPWRS.2023.3328158.

Digital Object Identifier 10.1109/TPWRS.2023.3328158

In the literature on frequency shifting-based component models, one shift frequency rather than multiple shift frequencies is considered. Moreover, it is common practice to associate the shift frequency with the ac grid frequency in the simulation of low-frequency transients. However, this approach should be extended in some cases where multi-carriers appear in different areas. As a typical example, the induction machine consisting of stator and rotor circuits is considered hereafter. The frequency of the quantities in the stator circuit is around the ac grid frequency, while the frequency of the quantities in the rotor circuit associated with the slip speed of the rotor is time-varying. It has been common to simulate induction machines in the phase domain [3], [4] by considering the frequency shifting for the stator circuit. However, with the frequency shifting for the rotor circuit neglected, the time step size may be limited due to the presence of the time-varying carrier. The accuracy of those models would benefit from also applying frequency shifting on the rotor side.

This letter addresses this issue. It is shown how multiple-frequency shifting is applied to the induction machine model. The setting of the shift frequencies is now two-dimensional instead of just being one-dimensional. The Fourier spectrum of the machine stator quantities is shifted by the ac grid frequency. The Fourier spectrum of the rotor quantities is shifted by the time-varying slip frequency. Case studies are performed to confirm benefits for simulation accuracy and efficiency.

## II. Multiple Frequency Shifting in Simulation

In the frequency shifting-based modeling techniques, all ac system quantities are represented through analytic signals instead of real signals based on Hilbert transform:

$$\underline{\boldsymbol{s}}(t) = \boldsymbol{s}(t) + \mathrm{j}\mathcal{H}\left[\boldsymbol{s}(t)\right] \tag{1}$$

with

$$\underline{\boldsymbol{s}}(t) = \left[s_1, s_2, \ldots, s_n\right]^{\mathrm{T}} \tag{2}$$

where $s_1, s_2, \ldots, s_n$ are the system quantities, $\boldsymbol{s}$ is the $n$-row vector representing system quantities, $\mathcal{H}$ denotes the Hilbert transform, underscore indicates an analytic signal. The Fourier spectra of quantities in the system may be different, as shown on the left of Fig. 1. The original real signals $\boldsymbol{s}(t)$ have negative frequency components. This is not the case for the corresponding analytic signals $\underline{s}_n(t)$, as shown in the middle of the Fig. 1.

Frequency shifting the vector $\underline{\boldsymbol{s}}(t)$ is performed as follows:

$$\mathcal{S}\left[\underline{\boldsymbol{s}}(t)\right] = \boldsymbol{\omega}(t) \cdot \underline{\boldsymbol{s}}(t) \tag{3}$$

with

$$\boldsymbol{\omega}(t) = \mathrm{diag}\left[\mathrm{e}^{-\mathrm{j}2\pi f_{\mathrm{s}1}(t)t}, \mathrm{e}^{-\mathrm{j}2\pi f_{\mathrm{s}2}(t)t}, \ldots, \mathrm{e}^{-\mathrm{j}2\pi f_{\mathrm{s}n}(t)t}\right] \tag{4}$$

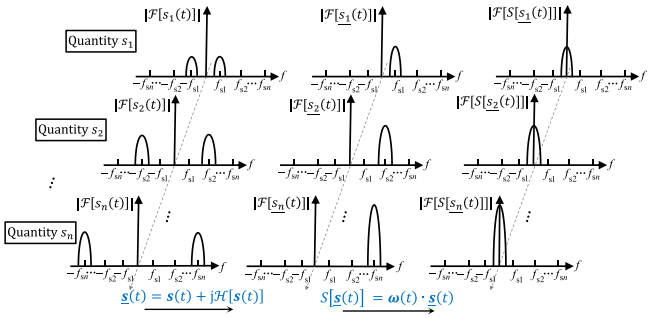


Fig. 1. Analytic signal processing and multiple frequency shifting.

where $\boldsymbol{\omega}$ is referred to as the frequency shifting matrix, which represents the multiple shift operations. Multi-dimensional shift frequencies can so be used in the simulation. The variables $f_{s1}, f_{s2}, \ldots, f_{sn}$ are the shift frequencies corresponding to the quantities $s_1$, $s_2, \ldots, s_n$. It should be noted that the shift frequency can be either constant or time-varying depending on the operating condition. Through the operation in (3), the spectra of system quantities are shifted by the frequency shifting matrix as shown on the right of Fig. 1. The maximum frequency of the shifted signal is lower than that of the original real bandpass signal. Thus, larger time step sizes can be chosen according to Nyquist criteria. The modeling technique is distinguished through the introduction of multiple and time-varying shift frequencies.

## III. Induction Machine Modeling Based on Multiple Frequency Shifting

In frequency shifting-based models, the quantities are represented by analytic signals for shift operations as presented in Section II. Using analytic signals, the voltage equations describing the behavior of the three-phase symmetrical induction machine is expressed in the phase domain as follows [3]:

$$\begin{bmatrix} \underline{\boldsymbol{v}}_{\text{abcs}}(t) \\ \underline{\boldsymbol{v}}_{\text{abcr}}(t) \end{bmatrix} = \frac{\mathrm{d}}{\mathrm{d}t} \begin{bmatrix} \underline{\boldsymbol{\lambda}}_{\text{abcs}}(t) \\ \underline{\boldsymbol{\lambda}}_{\text{abcr}}(t) \end{bmatrix} + \begin{bmatrix} \boldsymbol{R}_{\text{s}} & 0 \\ 0 & \boldsymbol{R}_{\text{r}} \end{bmatrix} \begin{bmatrix} \underline{\boldsymbol{i}}_{\text{abcs}}(t) \\ \underline{\boldsymbol{i}}_{\text{abcr}}(t) \end{bmatrix} \tag{5}$$

with

$$\begin{bmatrix} \underline{\boldsymbol{\lambda}}_{\text{abcs}}(t) \\ \underline{\boldsymbol{\lambda}}_{\text{abcr}}(t) \end{bmatrix} = \begin{bmatrix} \boldsymbol{L}_{\text{ss}} & \boldsymbol{L}_{\text{sr}}(\theta_{\text{r}}(t)) \\ \boldsymbol{L}_{\text{rs}}(\theta_{\text{r}}(t)) & \boldsymbol{L}_{\text{rr}} \end{bmatrix} \begin{bmatrix} \underline{\boldsymbol{i}}_{\text{abcs}}(t) \\ \underline{\boldsymbol{i}}_{\text{abcr}}(t) \end{bmatrix} \tag{6}$$

where $\underline{\boldsymbol{v}}_{\text{abcs}}$ and $\underline{\boldsymbol{v}}_{\text{abcr}}$ are the stator and rotor voltages, respectively; $\underline{\boldsymbol{i}}_{\text{abcs}}$ and $\underline{\boldsymbol{i}}_{\text{abcr}}$ are the stator and rotor currents, respectively; $\underline{\boldsymbol{\lambda}}_{\text{abcs}}$ and $\underline{\boldsymbol{\lambda}}_{\text{abcr}}$ are the stator and rotor flux linkages, respectively; $\boldsymbol{R}_{\text{s}}$ and $\boldsymbol{R}_{\text{r}}$ are stator and rotor resistances, respectively; $\boldsymbol{L}_{\text{ss}}$ and $\boldsymbol{L}_{\text{rr}}$ are the stator and rotor inductance matrices; $\boldsymbol{L}_{\text{sr}}$ and $\boldsymbol{L}_{\text{rs}}$ are the mutual inductance matrices; $\theta_{\text{r}}$ is the rotor position.

Multiplying both sides of (5) by the frequency shifting matrix and introducing the notation of (3) gives:

$$\begin{aligned} \mathcal{S}\begin{bmatrix} \underline{\boldsymbol{v}}_{\text{abcs}}(t) \\ \underline{\boldsymbol{v}}_{\text{abcr}}(t) \end{bmatrix} &= \mathrm{j}\boldsymbol{\omega}_{\text{mac}}(t)\mathcal{S}\begin{bmatrix} \underline{\boldsymbol{\lambda}}_{\text{abcs}}(t) \\ \underline{\boldsymbol{\lambda}}_{\text{abcr}}(t) \end{bmatrix} + \frac{\mathrm{d}}{\mathrm{d}t}\mathcal{S}\begin{bmatrix} \underline{\boldsymbol{\lambda}}_{\text{abcs}}(t) \\ \underline{\boldsymbol{\lambda}}_{\text{abcr}}(t) \end{bmatrix} \\ &+ \begin{bmatrix} \boldsymbol{R}_{\text{s}} & 0 \\ 0 & \boldsymbol{R}_{\text{r}} \end{bmatrix}\mathcal{S}\begin{bmatrix} \underline{\boldsymbol{i}}_{\text{abcs}}(t) \\ \underline{\boldsymbol{i}}_{\text{abcr}}(t) \end{bmatrix} \end{aligned} \tag{7}$$

with

$$\boldsymbol{\omega}_{\text{mac}}(t) = \begin{bmatrix} \boldsymbol{\omega}_{\text{sta}} & \boldsymbol{0} \\ \boldsymbol{0} & \boldsymbol{\omega}_{\text{rot}}(t) \end{bmatrix} \tag{8}$$

$$\boldsymbol{\omega}_{\text{sta}} = \text{diag}\left[\mathrm{e}^{-\mathrm{j}2\pi f_{\text{s1}} t}, \mathrm{e}^{-\mathrm{j}2\pi f_{\text{s1}} t}, \mathrm{e}^{-\mathrm{j}2\pi f_{\text{s1}} t}\right] \tag{9}$$

$$\boldsymbol{\omega}_{\text{rot}}(t) = \text{diag}\left[\mathrm{e}^{-\mathrm{j}2\pi f_{\text{s2}}(t) t}, \mathrm{e}^{-\mathrm{j}2\pi f_{\text{s2}}(t) t}, \mathrm{e}^{-\mathrm{j}2\pi f_{\text{s2}}(t) t}\right] \tag{10}$$

where $\boldsymbol{\omega}_{\text{mac}}$ is the frequency shifting matrix of the machine model; $f_{\text{s1}}$ is the stator shift frequency typically either 50 Hz or 60 Hz when tracking electromechanical transients; $f_{\text{s2}}$ is the rotor shift frequency which is equal to the slip frequency depending on the rotor speed.

Application of the trapezoidal integration method to (7) gives a difference equation:

$$\begin{aligned} &\mathcal{S}\begin{bmatrix} \underline{\boldsymbol{v}}_{\text{abcs}}(k) \\ \underline{\boldsymbol{v}}_{\text{abcr}}(k) \end{bmatrix} + \mathcal{S}\begin{bmatrix} \underline{\boldsymbol{v}}_{\text{abcs}}(k-1) \\ \underline{\boldsymbol{v}}_{\text{abcr}}(k-1) \end{bmatrix} \\ &= \mathrm{j}\begin{bmatrix} \boldsymbol{\omega}_{\text{sta}} & \boldsymbol{0} \\ \boldsymbol{0} & \boldsymbol{\omega}_{\text{rot}}(t) \end{bmatrix}\left(\mathcal{S}\begin{bmatrix} \underline{\boldsymbol{\lambda}}_{\text{abcs}}(k) \\ \underline{\boldsymbol{\lambda}}_{\text{abcr}}(k) \end{bmatrix} + \mathcal{S}\begin{bmatrix} \underline{\boldsymbol{\lambda}}_{\text{abcs}}(k-1) \\ \underline{\boldsymbol{\lambda}}_{\text{abcr}}(k-1) \end{bmatrix}\right) \\ &\quad + \frac{2}{\tau}\left(\mathcal{S}\begin{bmatrix} \underline{\boldsymbol{\lambda}}_{\text{abcs}}(k) \\ \underline{\boldsymbol{\lambda}}_{\text{abcr}}(k) \end{bmatrix} - \mathcal{S}\begin{bmatrix} \underline{\boldsymbol{\lambda}}_{\text{abcs}}(k-1) \\ \underline{\boldsymbol{\lambda}}_{\text{abcr}}(k-1) \end{bmatrix}\right) \\ &\quad + \begin{bmatrix} \boldsymbol{R}_{\text{s}} & 0 \\ 0 & \boldsymbol{R}_{\text{r}} \end{bmatrix}\left(\begin{bmatrix} \underline{\boldsymbol{i}}_{\text{abcs}}(k) \\ \underline{\boldsymbol{i}}_{\text{abcr}}(k) \end{bmatrix} + \mathcal{S}\begin{bmatrix} \underline{\boldsymbol{i}}_{\text{abcs}}(k-1) \\ \underline{\boldsymbol{i}}_{\text{abcr}}(k-1) \end{bmatrix}\right) \end{aligned} \tag{11}$$

where $\tau$ is the time step size, $k$ is the time step counter.

By insertion of analytic signals and rearrangement of (11), the following expressions for $\underline{\boldsymbol{v}}_{\text{abcs}}$ and $\underline{\boldsymbol{i}}_{\text{abcr}}$ are obtained:

$$\underline{\boldsymbol{v}}_{\text{abcs}}(k) = \boldsymbol{R}_{\text{s}}\underline{\boldsymbol{i}}_{\text{abcs}}(k) + \left(\mathrm{j}\boldsymbol{\omega}_{\text{sta}} + \frac{2}{\tau}\right)\underline{\boldsymbol{\lambda}}_{\text{abcs}}(k) + \underline{\boldsymbol{e}}_{\text{sh}}(k), \tag{12}$$

$$\begin{aligned} \underline{\boldsymbol{i}}_{\text{abcr}}(k) = &\left(\boldsymbol{R}_{\text{r}} + \left(\mathrm{j}\boldsymbol{\omega}_{\text{rot}}(k) + \frac{2}{\tau}\right)\boldsymbol{L}_{\text{rr}}\right)^{-1} \\ &\times \left(-\left(\mathrm{j}\boldsymbol{\omega}_{\text{rot}}(k) + \frac{2}{\tau}\right)\boldsymbol{L}_{\text{rs}}(\theta_{\text{r}}(k))\underline{\boldsymbol{i}}_{\text{abcs}}(k)\right. \\ &\left. + \underline{\boldsymbol{v}}_{\text{abcr}}(k) + \underline{\boldsymbol{e}}_{\text{rh}}(k)\right), \end{aligned} \tag{13}$$

with

$$\begin{aligned} \underline{\boldsymbol{e}}_{\text{sh}}(k) = &-\mathrm{e}^{\mathrm{j}2\pi f_{\text{s1}}(k)\tau}\underline{\boldsymbol{v}}_{\text{abcs}}(k-1) + \boldsymbol{R}_{\text{s}}\mathrm{e}^{\mathrm{j}2\pi f_{\text{s1}}(k)\tau}\underline{\boldsymbol{i}}_{\text{abcs}}(k-1) \\ &+ \left(\mathrm{j}\boldsymbol{\omega}_{\text{sta}} - \frac{2}{\tau}\right)\mathrm{e}^{\mathrm{j}2\pi f_{\text{s1}}(k)\tau}\underline{\boldsymbol{\lambda}}_{\text{abcs}}(k-1) \end{aligned} \tag{14}$$

and

$$\begin{aligned} &\underline{\boldsymbol{e}}_{\text{rh}}(k) \\ &= \mathrm{e}^{\mathrm{j}2\pi f_{\text{s2}}(k)\tau}\underline{\boldsymbol{v}}_{\text{abcr}}(k-1) \\ &\quad -\left(\boldsymbol{R}_{\text{r}} + \left(\mathrm{j}\boldsymbol{\omega}_{\text{rot}}(k) - \frac{2}{\tau}\right)\boldsymbol{L}_{\text{rr}}\right)\mathrm{e}^{\mathrm{j}2\pi f_{\text{s2}}(k)\tau}\underline{\boldsymbol{i}}_{\text{abcr}}(k-1) \\ &\quad -\left(\mathrm{j}\boldsymbol{\omega}_{\text{rot}}(k) - \frac{2}{\tau}\right)\boldsymbol{L}_{\text{rs}}(\theta_{\text{r}}(k-1))\,\mathrm{e}^{\mathrm{j}2\pi f_{\text{s2}}(k)\tau}\underline{\boldsymbol{i}}_{\text{abcs}}(k-1) \end{aligned} \tag{15}$$

From (6), the stator flux linkage may be expressed as:

$$\underline{\boldsymbol{\lambda}}_{\text{abcs}}(k) = \boldsymbol{L}_{\text{ss}}\underline{\boldsymbol{i}}_{\text{abcs}}(k) + \boldsymbol{L}_{\text{sr}}(\theta_{\text{r}}(k))\,\underline{\boldsymbol{i}}_{\text{abcr}}(k) \tag{16}$$

TABLE I
MACHINE PARAMETERS

| Machines | $S_B$/MW | $V_B$/kV | $X_s$/pu | $X_r$/pu | $X_m$/pu | $r_s$/pu | $r_r$/pu |
|---|---|---|---|---|---|---|---|
| Type 1 | 3 | 6 | 0.107 | 0.098 | 2.22 | 0.077 | 0.079 |
| Type 2 | 3 | 6 | 0.094 | 0.163 | 2.80 | 0.035 | 0.048 |

Substitution of (13) and (16) in (12) gives the following Thevenin equivalent:

$$\underline{\boldsymbol{v}}_{\text{abcs}}(k) = \underline{\boldsymbol{R}}_{\text{eq}}(k)\underline{\boldsymbol{i}}_{\text{abcs}}(k) + \underline{\boldsymbol{e}}_{\text{h}}(k), \tag{17}$$

with

$$\begin{aligned}\underline{\boldsymbol{R}}_{\text{eq}}(k) = \underline{\boldsymbol{R}}_{\text{s}} &+ \left(\text{j}\boldsymbol{\omega}_{\text{sta}} + \frac{2}{\tau}\right)\boldsymbol{L}_{\text{ss}} - \left(\text{j}\boldsymbol{\omega}_{\text{rot}}(k) + \frac{2}{\tau}\right) \\ &\times \left(\text{j}\boldsymbol{\omega}_{\text{sta}} + \frac{2}{\tau}\right)\boldsymbol{L}_{\text{sr}}\left(\theta_{\text{r}}(k)\right) \\ &\times \left(\boldsymbol{R}_{\text{r}} + \left(\text{j}\boldsymbol{\omega}_{\text{rot}}(k) + \frac{2}{\tau}\right)\boldsymbol{L}_{\text{rr}}\right)^{-1}\boldsymbol{L}_{\text{rs}}\left(\theta_{\text{r}}(k)\right),\end{aligned} \tag{18}$$

$$\begin{aligned}\underline{\boldsymbol{e}}_{\text{h}}(k) = &\left(\text{j}\boldsymbol{\omega}_{\text{sta}} + \frac{2}{\tau}\right)\boldsymbol{L}_{\text{sr}}\left(\theta_{\text{r}}(k)\right) \\ &\times \left(\boldsymbol{R}_{\text{r}} + \left(\text{j}\boldsymbol{\omega}_{\text{rot}}(k) + \frac{2}{\tau}\right)\boldsymbol{L}_{\text{rr}}\right)^{-1} \\ &\left(\underline{\boldsymbol{e}}_{\text{rh}}(k) + \underline{\boldsymbol{v}}_{\text{abcr}}(k) + \underline{\boldsymbol{e}}_{\text{sh}}(k)\right)\end{aligned} \tag{19}$$

where $\underline{\boldsymbol{R}}_{\text{eq}}$ is the equivalent resistance matrix, $\underline{\boldsymbol{e}}_{\text{h}}$ is the total history term. In the presented model, there are two shift frequencies: $f_{s1}$ and $f_{s2}$. The shift frequency $f_{s1}$ can be set to the ac grid frequency to eliminate the ac carrier on the stator. The shift frequency $f_{s2}$ is a function of the rotor speed and thus time-varying. The purpose of the introduction of $f_{s2}$ is to eliminate the carrier on the rotor side. This feature distinguishes the models from [3] and [4] where no frequency shifting is applied on the rotor side. In [3] and [4], the shift frequency $f_{s2}$ is not available. This corresponds to always having $f_{s2}$= 0 Hz in the presented model. Moreover, the shift frequencies $f_{s1}$ and $f_{s2}$ may be set to zero when fault studies are of interest.

## IV. CASE STUDIES

A test system covering a high-slip induction machine connected directly to an ideal voltage source is used to examine the results provided by the proposed machine model. The focus of this test system is on the investigation of numerical properties of the individual machine model. The parameters of type 1 of tested machine from [5] are given in Table I.

It is assumed that the machine is initially running at rated speed in the steady state. The rotor speed is ramped down by 10% of rated value within 0.5 s to 1.5 s and ramped up by 5% of rated value within 2.5 s to 3 s. In this test, low-frequency transients are present. To allow for accurate and efficient simulation of low-frequency transients, multiple shift frequencies are used for the proposed model. The shift frequency $f_{s1}$ is set equal to the grid frequency of 60 Hz. The shift frequency $f_{s2}$ is set adaptively to the slip frequency. The time step size is set to 20 ms. For the purpose of comparison, the case of non-adaptive constant shift frequency settings is considered as e.g., performed in [3] or [4]. The time step size for this case is also set to 20 ms. In accordance with [3], the reference solution was obtained using the dq model implemented in MATLAB/Simulink and solved with the Runge-Kutta 4th order method with a time step size of 1 $\mu$s.

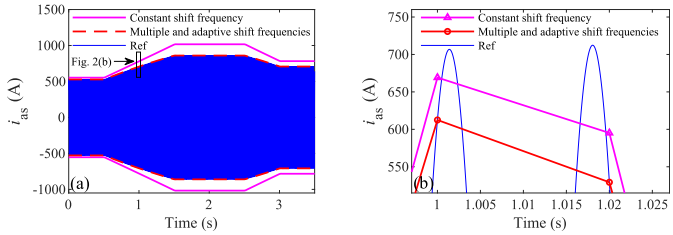


Fig. 2. Phase a stator current $i_{as}$.

TABLE II
TWO-NORM ERROR OF STATOR AND ROTOR CURRENT UNDER VARIOUS TIME STEP SIZES

| | Constant shift frequency | | Multiple and adaptive shift frequencies | |
|---|---|---|---|---|
| Time step | Stator current | Rotor current | Stator current | Rotor current |
| 1 ms | 0.0419% | 0.0434% | 0.0367% | 0.0409% |
| 2 ms | 0.1211% | 0.1265% | 0.0367% | 0.0410% |
| 5 ms | 0.7656% | 0.8474% | 0.0368% | 0.0410% |
| 10 ms | 3.1858% | 3.5536% | 0.0397% | 0.0444% |
| 20 ms | 14.8287% | 16.5746% | 0.0409% | 0.0474% |

The results of the comparison of the phase a stator currents are shown in Fig. 2. The frequency shifting-based models support the tracking of envelope waveforms. As shown in Fig. 2(a), the envelope produced by the proposed model accurately touches the instantaneous amplitudes as observed with the reference solution. To focus on details, zoomed-in views of stator currents are displayed in Fig. 2(b). The real parts of the shifted analytic signals represent the time domain instantaneous values shown using circles. The latter may be used to further examine the accuracies of envelope waveforms produced by different shift frequency settings. From Fig. 2(b), it can be seen that the results obtained with the multiple and adaptive shift frequency setting are in good agreement with the reference curve. For constant shift frequency settings, the deviations of the simulation results from the reference are visibly larger.

The 2-norm cumulative relative errors are used to further investigate the accuracies of various shift frequency settings:

$$\varepsilon\left(i_{\text{as}}\right) = \frac{||i_{\text{as,ref}} - i_{\text{as}}||_2}{||i_{\text{as,ref}}||_2} \times 100\% \tag{20}$$

The 2-norm errors of stator current and rotor current of the adaptive shift frequency are 0.0409% and 0.0474%. The errors of stator current and rotor current are 14.8287% and 16.5746%, respectively, for constant shift frequency setting $f_{s1}$ = 60 Hz. The improved accuracy is attributed to the operation of multiple and adaptive frequency shifting.

The errors for adaptive setting of the shift frequency are close to zero and remain nearly constant even at rising time step sizes, as shown in Table II. At a constant shift frequency setting, the errors are shown to rise as the time step size increases. At time step size of 1 ms, the errors of stator current and rotor current for constant shift frequency setting are 0.0419% and 0.0434%, respectively. To achieve similar accuracy, the time step size for

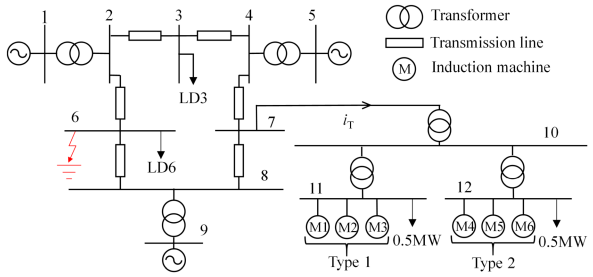


Fig. 3. One-line diagram of the multi-machine system.

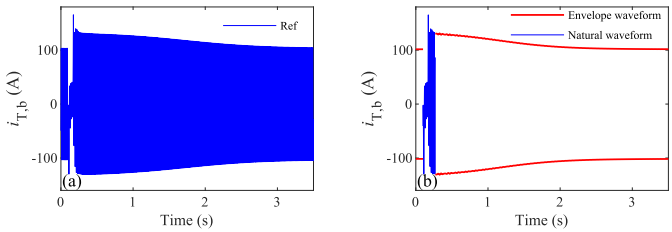


Fig. 4. Phase b current of $i_T$; (a) reference solution in PSCAD; (b) multi-scale simulation results obtained with the proposed model.

the model with multiple and adaptive shift frequencies may be increased to 20 ms.

To evaluate the computational efficiency, the proposed model and the model with constant shift frequency are implemented using standard C language. The models are executed on a personal computer with an Intel Core i5-10400F, 2.90-GHz processor and 16 GB RAM. The CPU times per time step required by the proposed model and the model with constant shift frequency are 0.396 $\mu$s and 0.262 $\mu$s, respectively. Taking into account both computation time per step and the used time step size, the simulation efficiency with multiple and adaptive shift frequencies is improved by a factor of (20 ms)·(0.262 $\mu$s)/(1 ms)/(0.396 $\mu$s) $\approx$ 13.2 as compared to that with constant shift frequency.

To further illustrate the value introduced by the proposed method, an example of multi-scale simulation of a multi-machine system for a three-phase fault is considered. The test system is shown in Fig. 3. A distribution network consisting of 6 induction machines with rated load torque is connected to the WSCC 9-bus system at bus 7. The parameters of the test system and machines can be referred to from [3] and [5]. At $t =$ 0.1 s, a three-phase-to-ground fault occurs at bus 6. The fault is cleared after four cycles. The test system is also modeled using PSCAD with a small time step size of 10 $\mu$s to provide reference solutions. For purposes of comparison, the model which only considers the frequency shifting on the stator side as in [3] is also included in the simulation. The simulation results are depicted in Fig. 4 and Fig. 5(a).

At the beginning of the simulation, the system is running in the steady state. The envelope waveforms are tracked at $\tau = 20$ ms. Multiple shift frequencies are used for the proposed machine model. The shift frequencies $f_{s1,M1}, \ldots, f_{s1,M6}$ are set equal to 60 Hz to eliminate the ac carriers on the stator. The shift frequencies $f_{s2,M1}, \ldots, f_{s2,M6}$ are set equal to the slip frequencies of different machines M1, $\cdots$, M6 to eliminate the carriers on the rotor, as shown in Fig. 5(b). From $t = 0.1$ s, electromagnetic transients appear due to the occurrence of fault.

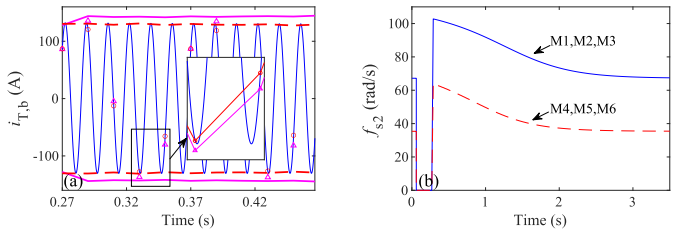


Fig. 5. Phase b current of $i_T$ and shift frequency $f_{s2}$; (a) zoomed-in view of $i_{T,b}$ during the period of electromechanical transients; solid light: reference solution; circles and dashed bold: natural waveform and envelope waveform obtained with the proposed model; triangles and solid bold: natural waveform and envelope waveform obtained with the model only considering the frequency shifting on the stator side; (b) time-varying setting of shift frequency $f_{s2}$ of different machines.

Then, no frequency shifting is applied and all shift frequencies are set to zero. Natural waveforms are tracked at $\tau = 10$ $\mu$s. As the electromagnetic transients damp out, multiple frequency shifting resumes at $t = 0.27$ s. The envelope is tracked with a time step size of 20 ms. As observed in Fig. 4 and Fig. 5(a), the multi-scale simulation results obtained with the proposed model closely match reference solution and are more accurate than that obtained with the model which neglects the frequency shifting for the rotor side.

## V. Conclusion

In this letter, the multiple frequency shifting theory is developed, implemented and validated. The presented work is distinguished through three contributions. First, the frequency shifting modeling methodology is extended to accommodate the components containing multi-carriers. Through the multi-dimensional and time-varying setting of shift frequencies, ac carriers are eliminated, which enables accurate and efficient simulation of low-frequency transients. Second, it was shown how the method can be applied in the modeling of induction machine. The Fourier spectra of stator quantities are shifted by the ac grid frequency, while the Fourier spectra of rotor quantities are shifted adaptively by the time-varying slip frequency. Third, the performance is validated through case study. The results show that the use of multiple and adaptive shift frequency settings is beneficial in the simulation of induction machine and provides more accurate solution compared to the use of constant shift frequency settings at large time step sizes.

## References

[1] K. Strunz, R. Shintaku, and F. Gao, "Frequency-adaptive network modeling for integrative simulation of natural and envelope waveforms in power systems and circuits," *IEEE Trans. Circuits Syst. I*, vol. 53, no. 12, pp. 2788–2803, Dec. 2006.

[2] P. Zhang, J. R. Martí, and H. W. Dommel, "Shifted-frequency analysis for EMTP simulation of power-system dynamics," *IEEE Trans. Circuits Syst. I*, vol. 57, no. 9, pp. 2564–2574, Sep. 2010.

[3] Y. Xia and K. Strunz, "Multi-scale induction machine model in the phase domain with constant inner impedance," *IEEE Trans. Power Syst.*, vol. 35, no. 3, pp. 2120–2132, May 2020.

[4] P. Zhang, J. R. Martí, and H. W. Dommel, "Induction machine modeling based on shifted frequency analysis," *IEEE Trans. Power Syst.*, vol. 24, no. 1, pp. 157–164, Feb. 2009.

[5] "IEEE task force on load representation for dynamical performance: Standard load models for power flow and dynamic performance simulation," *IEEE Trans. Power Syst.*, vol. 10, no. 3, pp. 1302–1313, Aug. 1995.